Journal of
Composites Science

MDPI

Article

Composite Overwrapped Pressure Vessel Design Optimization Using Numerical Method

Yohannes Regassa [1,*], Jema Gari [2] and Hirpa G. Lemu [3,*]

[1] Mechanical Engineering Department, College of Electrical and Mechanical Engineering, Addis Ababa Science and Technology University, Addis Ababa P.O. Box 16417, Ethiopia
[2] Department of Mechanical Engineering, College of Engineering and Technology, Mettu University, Mettu P.O. Box 318, Ethiopia
[3] Department of Mechanical and Structural Engineering and Materials Science, Faculty of Science and Technology, University of Stavanger, P.O. Box 8600 FORUS, N-4036 Stavanger, Norway
* Correspondence: yohannes.regassa@aastu.edu.et (Y.R.); hirpa.g.lemu@uis.no (H.G.L.)

Abstract: Composite Overwrapped Pressure Vessels (COPVs) are widely used in fields including aeronautics and by companies such as SpaceX to hold high pressure fluids. They are favored for these applications because they are far lighter than all-metal vessels, although they demand special design, manufacturing, and testing requirements. In this study, finite element modeling was used to conducted stress and damage assessments on a composite overwrapped pressure vessel that has a 4 mm thick aluminum core cylinder. To develop the optimum COPV, the lamina sequences, thickness, and fiber winding angle were considered. The relationship between these variables and the composite-overwrapped structure's maximum burst pressure bearing capacity was assessed. The ABAQUS composite modeler was used to design and generate 14 models of COPVs from carbon fiber/epoxy plies with a consistent thickness of 6.5 mm and various fiber angle orientations. The effects of the ply stacking order were analyzed by the finite element analysis approach for all designed models, which had 13 layers of uniform thickness but a varying fiber orientation. A ply stacking sequence of [55°, −55°] PP winding pattern had an optimum COPV design profile, with a burst pressure bearing capacity of 24 MPa. The stress–strain distribution along the geometry of the COPV was also obtained using the finite element method, and it was found that the distribution is uniform over the surface of the COPV and that its peak values are found towards the polar boss section of the COPV. Extreme stress gradients were noticed when the boss nears its geometrical transition to the dome phase. This factor is evident from the change in the ply thickness caused by the overlapped fiber orientation. The results obtained from this study are useful for the design and application of composite overwrapped pressure vessels.

Keywords: burst pressure; composite overwrapped pressure vessel; failure criteria; finite element method; optimal winding angle; pressure vessel

Citation: Regassa, Y.; Gari, J.; Lemu, H.G. Composite Overwrapped Pressure Vessel Design Optimization Using Numerical Method. *J. Compos. Sci.* **2022**, *6*, 229. https://doi.org/10.3390/jcs6080229

Academic Editors: Salvatore Brischetto and Francesco Tornabene

Received: 30 June 2022
Accepted: 2 August 2022
Published: 5 August 2022

1. Introduction

The introduction of high-performance Kevlar- and carbon fiber-based composite materials accompanied with the optimum design of fiber alignment has enabled the production of filament wound composite overwrapped pressure vessels (COPV) as a vital energy storage capacity type of equipment per optimal unit mass [1]. COPVs are containers that are used to hold a liquid under pressure. Based on the composite coverage, there are many forms of composite pressure vessels (CPV). Among these categories, the type III pressure vessel is made up of a filament wound aluminium lining and a composite overwrap [2]. A study of early COPV design reported in [3] provides an introduction to the mechanical difficulties of COPVs. High-performance COPVs' structural designs are aimed at operations demanding fiber stress values of 60 to 70% of maximum stress. The composite strains

exceed the matrix-cracking and -crazing limit at these stress levels. As a result, liners are needed to obtain leak-free structures [3,4].

Elastomers and thin metallic liners were researched [5] extensively early on because of their potential to store a large amount of energy. However, the elastomers tested were unsuitable for high-pressure gas applications due to tearing and blistering. To eliminate the bending or creasing of thin metal liners during unloading stages, they must be glued to the composite overwrap [6]. Therefore, COPV design and analysis should consider the interaction between the liner and fiber overwrap. Soft aluminum or ductile materials with limited load-sharing capacity have commonly been used as COPV liners [7].

Plastics have been used as liner materials in recent COPV designs to reduce the weight of the structures [2,8]. In most cases, the fiber is applied as a strip of several fibers that is passed through a liquid resin. The vessel liner and the impregnated-fibers strip-distribution tip operate with respect to one another to wrap the fiber on the liner in the required shape. For the construction of the cylindrical vessel, the fiber winding is usually placed in both lengthwise (spiral) and circular (hoop) wraps [9]. The filament winding method for composite pressure vessel production entails several critical steps, including determining the resin composition, fiber design, the wrapping tension, and the wrap arrangement in relation to the liner's axis and requires the curing temperature of the impregnated fiber to be at high within the given time [10]. The design of all the vessels should consider, for the sake of its service, the testing pressures, external stresses due to mechanical impacts and chemical reactions, lifespan, and the safety factor set both for the static and dynamic working scenarios of the vessel structures [11]. Figure 1a depicts a traditional metal-based pressure vessel production method, whereas Figure 1b,c depict the filament winding process for Type II-IV COPV, which employ a continuous filament of reinforcement material wound at varying layers and requiring patterns over a rotating mandrel to produce type II, III, and IV composite overwrapped pressure vessels that can be used for energy storage [1,2,8].

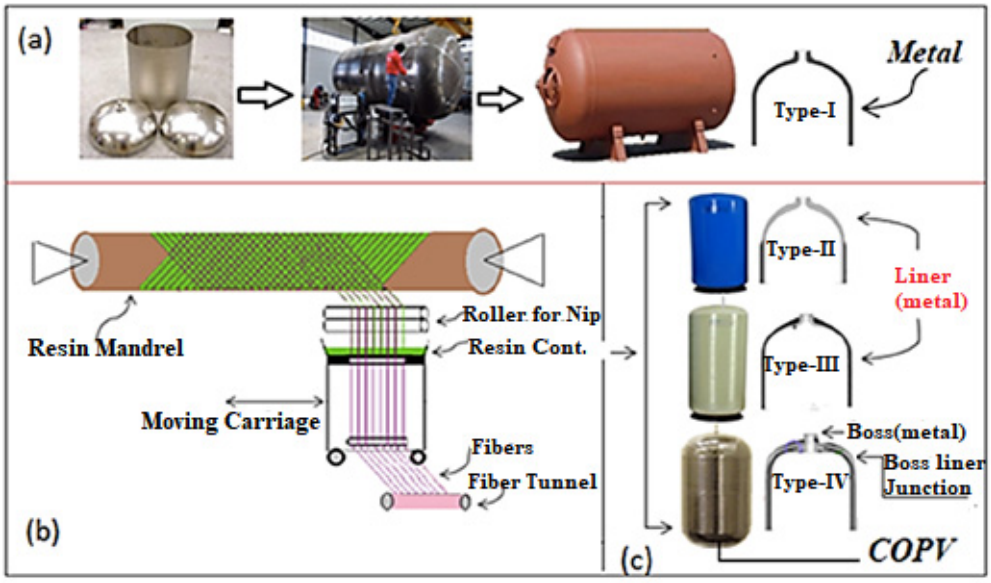

Figure 1. (**a**) Type-I Pressure vessel production method, (**b**) Filament winding layout for COPV production (reproduced from [12], an open access article distributed under the terms of the Creative Commons CC-BY license, which permits unrestricted use, distribution, and reproduction), and (**c**) Geometrical overview of vessels type II-IV (Reproduced with permission from [13]; copyright © 2017 Elsevier Ltd., Amsterdam, The Netherlands).

Type I cylindrical vessels are designed to store hydrogen gas at 20–30 MPa and are built entirely of metal. They have a low mass storage efficiency, which is about 1% of the hydrogen stored, and are challenged with fulfilling the stipulated specifications for

hydrogen energy storage applications. For on-board storage in vehicles, the European goal for weight efficiency is designated at 4.8 wt% of hydrogen stored in the system [14]. This goal can be achieved with a carbon fiber composite type III or type IV COPV with a working pressure of 70 MPa [14,15].

As manufacturing technology progresses, pressure vessel applications have spread swiftly worldwide [16]. Nowadays, there are various commercial algorithms that have used the mandrel's form as the primary data to generate filament winding paths. According to the work reported in [15], a more complex path-generating approach was studied in order to improve the end performance of the product. The method considers the mandrel's changing form as a result of the ply's uneven thickness distribution from earlier winding forms. The other approach necessitates the use of sophisticated machines and requires the purchase of commercial software for path development in order to achieve the optimum design of the COPV [15,16].

The stress and deformation distribution in actual COPV structures can be non-uniform due to a variety of variables ([11,12]) including the liner's relative stiffness to the overwrap, the liner–overwrap interface slip characteristics, and the occurrence of incompatible curvature changes. In regions where the liner thickness is constant, the overwrap may appear to act as an elastic base that cradles the liner [16]. For cylinders subjected to internal pressure, numerical analyses have been used to assess the stress and damage of COPVs with aluminum liners [6,16]. Both the tension and compression of the fiber and the matrix have been investigated as failure modes for the composite material [10]. This research investigated the impact of damage evolution on the burst pressure and auto-frettage pressure. When the cylinder was subjected to the service pressure, the matrix fracture damage was discovered on the head of the vessel and fiber tensile damage on the central section of the cylinder. The study also indicated that auto-frettage has a minor impact on stress amplitude but a big impact on mean stress.

To optimize pressure vessel design parameters, an analytical solution and numerical analysis in finite element analysis (FEA) were applied [9]. The materials chosen for the comparison in this study were stainless steel and fiber-reinforced composite materials. For a specific lay-up configuration, the thickness of the pressure vessel is determined by the fiber orientation and material type. In comparison to stainless steel pressure vessels, the composite pressure vessel has better weight savings. The damage evolution and failure strength of composite hydrogen storage tanks under internal pressure were predicted using a 3D parametric finite element model [17], where the FEA was limited to the cylindrical portion of the pressure vessel. The cylinder was made of 10 layers of carbon fiber/epoxy composite material and the liner was made of 6061-T6 aluminum alloy. According to the studies reported in [6,9], the structural damage was predicted based on four failure criteria, among which the Tsai–Wu failure criteria were found to be the most accurate.

Pressure vessels with a thermoplastic liner and glass filament wound reinforcements were studied in [13]. Accordingly, the mechanical behavior of pressure vessels under internal pressure to failure was investigated using the commercial software ABAQUS. The FEA results were then compared with experimental results. The advancement of filament winding technology is boosting composite material use in emerging COPV markets [17].

For years, filament winding has been used to manufacture axisymmetric fiber-reinforced polymer structures such as pipes, pressure tanks, pipe fittings, and drive shafts [10]. Robotic advancements have also enabled the production of composite components with more complex shapes [18]. Compared to traditional all-metal structures such as pressure vessels, filament winding can produce structures with extremely high stiffness-to-weight and strength-to-weight ratios [12]. The aerospace industry benefits from rocket propellant tanks and solid rocket motor casings, while the automotive industry benefits from high-pressure fuel storage tanks for hydrogen-powered cars [19]. The design optimization of the composite pressure vessel was studied by FEA and empirical validation with respect to a variety of structural applications to acquire the optimum winding angles of composite overwrapped pressure vessels [20]. Due to the complicated nature of the composite structure, an experi-

mental verification of FEM derived results is also essential. In the work reported in [21], research was conducted utilizing the conventional laminated plate and Tsai–Wu failure theories. They observed that the optimal inter-ply angles varied with the type of material, with values of 52.1° and 54.1°. Another study reported in [22] was performed to visualize the problems of internal pressure single-sided composite pipe optimization. They looked at E-glass, carbon, and Kevlar fiber-reinforced composites and found that three winding orientations, 53.2°, 54.3°, and 54.9°, were optimal.

Another study [23] was performed on the cylindrical section of four-layer vessels considering both the hoop and polar winding angle. The burst pressure was estimated as a function of the different fiber orientation angles. They determined that the orientation angle $\alpha \pm 45°$ was the best among the possible fiber orientation angles studied.

A comprehensive literature study on the effects of the fiber winding angle, the ply sequencing pattern, and the ply thickness for composite overwrapped pressure vessels subjected to internal pressure stress and damage analysis indicates that more studies are still needed despite the significant prior studies focusing on the impact of various loads on the mechanical damage of vessels made of composites. Furthermore, from the reported literature, limited emphasis has been placed on the parameters' effect on the geometrical profile of COPV. To address some of the observed limitations in the literature, the objective of the current study is to examine the design of composite overwrapped pressure vessels to provide optimized variables with a focus on two major issues: (1) performing FEA on a composite overwrap pressure vessel that has been designed with a variety of layers and orientations to withstand a maximum burst pressure, and (2) examining the stress and damage characteristics of COPV designs with a uniform fiber angle orientation but different ply sequences.

2. Materials and Methods

Carbon fiber is commonly used in construction of both computational and physical models of COPV because it has a high-modulus of elasticity and high-strength with a low coefficient of thermal expansion as well as high fatigue strength [24]. Since the COPV has an inner layer made of aluminum alloy, the AL6061 physical properties were used to model it. The physical properties of the used carbon fiber reinforced polymer composite (CFRP) and AL6061 to model the COPV were adopted from [25,26], whose values are shown in Table 1.

Table 1. Physical property values of Aluminum linear and CFRP (T800S and TCRUF 3325-95).

	Property	Units	Value
Aluminum (AL6061)	Density	(kg/m^3)	1570
	Young's modulus	GPa	74.12
	Poisson's ratio (ν)	-	0.3
	Ultimate shear strength	GPa	0.6
Elastic	Young's modulus in direction 1 (E1)	GPa	176.8
	Young's modulus in direction 2 (E2)	GPa	10.3
	Poisson's ratio in direction 12 (ν12)	-	0.23
	Shear modulus in direction 12 (G12)	MPa	4.8
Hashin's parameters	Tensile strength in direction 1(X^T)	GPa	3.3
	Compressive strength in direction 1 (X^C)	GPa	1.7
	Tensile strength in direction 2 (Y^T)	GPa	0.096
	Compressive strength in direction 2 (Y^C)	GPa	0.289
	Shear strength in direction 1 (S^L)	GPa	0.096
	Shear strength in direction 2 (S^T)	MPa	0.096
Damage Evolution	Longitudinal Tensile Fracture Energy (G^{lt})	MJ/mm^2	984.778
	Longitudinal Compressive Fracture Energy (G^{lc})	MJ/mm^2	277.9966
	Transverse Tensile Fracture Energy (G^{tt})	MJ/mm^2	7.02575
	Transverse Compressive Fracture Energy (G^{tc})	MJ/mm^2	117.694

2.1. Analytical Study of the Composite Overwrapped Pressure Vessel

The geometrical representations of the studied pressure vessel, as well as the accompanying nomenclature, are shown in Figure 2. According to shell theory, the fiber path must be satisfied for balanced stress levels in the dome region. If the strains in the shell are modest enough, it should be ignored in comparison to unity [26].

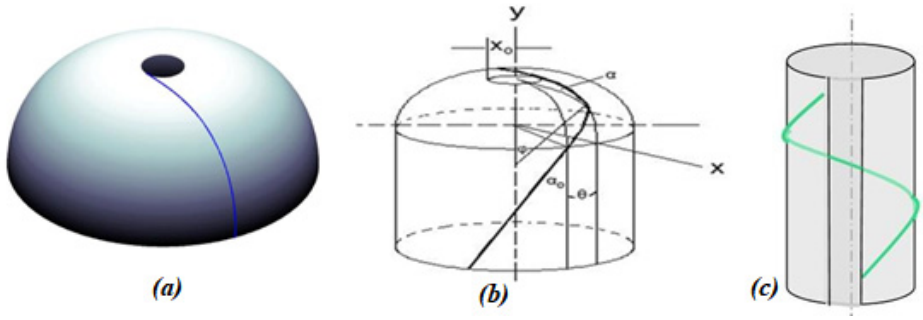

Figure 2. COPV: (**a**) fiber geodesic path on dome, (**b**) schematic view of vessel coordinates, and (**c**) fiber path on cylinder.

The normalized dome profile of the pressure vessel is plotted using y as a function of the axial coordinate x yielding an elliptic integral of the third kind [26].

$$y = -\int \frac{x^3 d_x}{\left[(1-x^2)(x^2-a_1)(x^2-a_2)\right]^{1/2}} + C \tag{1}$$

where: $a_1 = \frac{1}{2}\left[\left(\frac{1+4{x_o}^2}{1-{x_o}^2}\right) - 1\right]$ and $a_2 = -\frac{1}{2}\left[\left(\frac{1+4{x_o}^2}{1-{x_o}^2}\right)^{1/2} + 1\right]$.

The constant of integration is evaluated from the fact that $y = 0$ when $x = 1$.

Integration of Equation (1) will produce the coordinates of the dome contour geometry. The initial winding angle of COPV is calculated using the relation in Equation (2) that relates to the non-geodesic winding method [27].

$$\alpha(\mathrm{R}) = \sin^{-1}\left(\frac{\mathrm{R_0}}{\mathrm{R}}\right) \pm \delta\left(\frac{\mathrm{R}-\mathrm{R_0}}{\mathrm{R_{tl}}-\mathrm{R_0}}\right)^{\mathrm{n}} \tag{2}$$

where R is the radial distance from the centerline to a point in the layer, $\mathrm{R_0}$ is the radius of the polar axis, and $\mathrm{R_{tl}}$ is the radius at the dome–cylinder tangent line. The exponent n controls the variation from the tangent line to the turnaround point [28].

$$\mathrm{N_\varnothing} = \frac{\mathrm{PR}}{2},\ \mathrm{N_\theta} = \mathrm{PR} \tag{3}$$

Axial and hoop stresses can be calculated as in Equation (4):

$$\sigma_{\mathrm{axial}} = \frac{\mathrm{N_\varnothing}}{t} = \frac{\mathrm{PR}}{2t},\ \sigma_{\mathrm{hoop}} = \frac{\mathrm{N_\theta}}{t} = \frac{\mathrm{PR}}{t} \tag{4}$$

According to [27], the thickness of the filament wound reinforcement at each point of the dome is obtained using Equation (5):

$$t = \frac{x_{cyl}}{x}\frac{\cos\alpha_{cyl}}{\cos\alpha(R)}t_{cyl} \tag{5}$$

where
α_{cyl} = winding angle at cylinder or dome junction;
t_{cyl} = thickness of composite at cylinder dome juncture;
x_{cyl} = radius at cylinder dome juncture.

Barlow's equation, Equation (6), is also used to determine the thickness of the cylindrical shell of the inner linear [29]:

$$T = P_B \times \frac{D}{2 \times \sigma_u} \tag{6}$$

where P_B is the burst pressure of the liner in MPa, σ_u is the ultimate strength of the material in MPa, T is the thickness of pressure vessel in mm, and D is the inner diameter of pressure vessel in mm.

Windenburg and Trilling Equation (Equation (7)) is used to determine composite shell critical pressure [28]. Accordingly, the critical pressure P_{cr} can be found by considering the thickness of the shell (t), diameter of the cylindrical shell (d), length (spacing) between the stiffeners (l), Young's Modulus (E), and Poisson's ratio (ν) as follows:

$$P_{cr} = \frac{2.42E\left[\frac{t}{d}\right]^{2.5}}{\left[1-\nu^2\right]^{0.75}\left[\frac{l}{d} - 0.45\left[\frac{t}{d}\right]^{0.5}\right]} \tag{7}$$

According to maximum shear stress theory of failure ([28–31]), material failure is predicted when its maximum allowable shear stress reaches the stress at which it would yield in a tensile test, and this is expressed as

$$\tau_{\max} = \frac{S_{sy}}{fs} = \frac{\sigma_1 - \sigma_2}{2} \tag{8}$$

This theory can also be used to determine the wall thickness (t) of the inner liner aluminum cylinder of inner diameter D_i subjected to internal pressures (P_i), which is given by:

$$t = \frac{D_i}{2}\left[\sqrt{\frac{\tau}{(\tau - P_i)}} - 1\right] \tag{9}$$

The Hashin failure criterion, which comprises four typical failure modes, the matrix tension and compression, the fiber tension and compression, and the initiation of damage to the composite layers, was used in this study to forecast failure [10].

$$F_f^t = \left(\frac{\sigma_1}{X_T}\right)^2 + \alpha\left(\frac{\sigma_6}{S_L}\right)^2 \text{ Fiber tension } (\sigma_1 \geq 0) \tag{10}$$

$$F_f^c = \left(\frac{\sigma_1}{X_c}\right)^2 \text{ Fiber compression } (\sigma_1 < 0) \tag{11}$$

$$F_m^t = \left(\frac{\sigma_2}{Y_T}\right)^2 + \left(\frac{\sigma_6}{S_L}\right)^2 \text{ Matrix tension } (\sigma_2 \geq 0) \tag{12}$$

$$F_m^c = \left(\frac{\sigma_2}{2S_T}\right)^2 + \left[\left(\frac{Y^C}{2S_T}\right)^2 - 1\right]\frac{\sigma_2}{Y_c} + \left(\frac{\sigma_6}{S_L}\right)^2 \text{ Matrix compression } (\sigma_2 < 0) \tag{13}$$

According to Tsai–Wu failure theory [32], delamination characteristics of the composite lamina that are subjected to plane stress conditions can be determined using Equations (14) and (15)

$$F_1\sigma_{11} + F_2\sigma_{22} + F_{11}\sigma_{11}^2 + F_{22}\sigma_{22}^2 + F_{66}\sigma_{12}^2 + 2F_{12}\sigma_{11}\sigma_{22} \tag{14}$$

where F_1, F_2, F_{11}, F_{22}, F_{12}, and F_{66} are determined based on the used materials strength parameters as formulated in Equation (15).

$$F_1 = \frac{1}{X_t} - \frac{1}{X_c}, F_2 = \frac{1}{Y_t} - \frac{1}{Y_c}, F_{11} = \frac{1}{X_t X_c}, F_{22} = \frac{1}{Y_t Y_c}, F_{12} = -\frac{1}{2}\sqrt{F_{11}F_{22}}, F_{66} = \frac{1}{S^2} \tag{15}$$

2.2. Finite Element Modeling of Composite Pressure Vessel

The pressure vessel model was created using the composite modeler of ABAQUS software using the steps shown in Figure 3, and the finite element analysis was completed using ABAQUS standard/explicit model. The required vessel profile was created as a full quarter model (90-degree sweep) using a cylindrical coordinate system with a 5-segment shell element. After that, an ABAQUS/CAE package was also used to generate the pressure vessel geometry, load-sharing metallic liner, and composite overwrap.

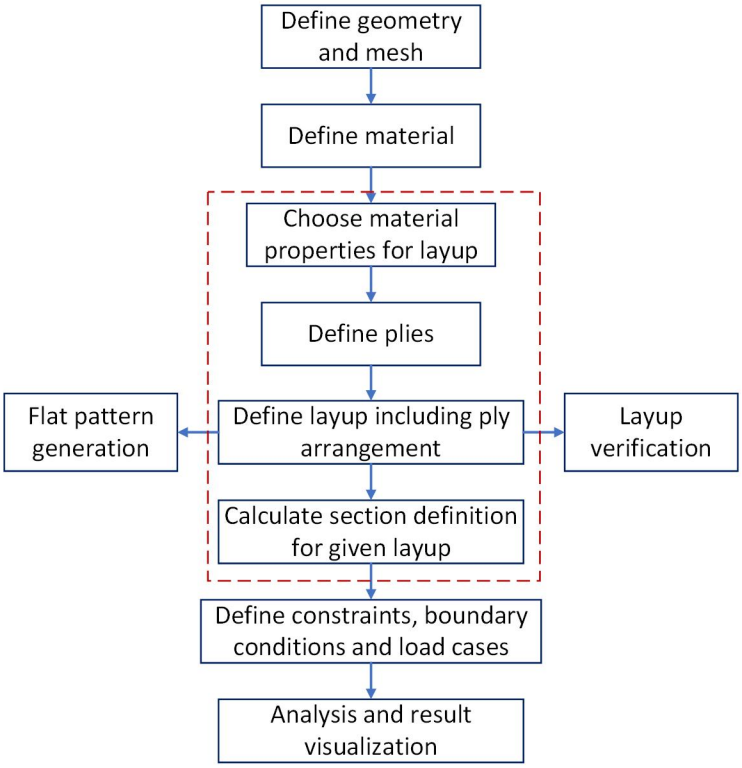

Figure 3. Modal analysis steps used in ABAQUS/CAE composite modeler.

The overall geometrical shape configuration of the inner linear and pressure vessel was determined as ASTMD 2585 standard for COPV, which was adopted from [33]. Accordingly, the vessel was made with a 240 mm length and 145 mm diameter, with an inner aluminum layer that was 4 mm thick. Using dome shape estimations, the geometry of the vessel was then plotted. However, developers can specify such a geometry after creating the CAD model and importing it as a part drawing by the provided analytical data. Figure 4a–c show the linear geometrical description, the 3D model, and stack sequence profiles, respectively.

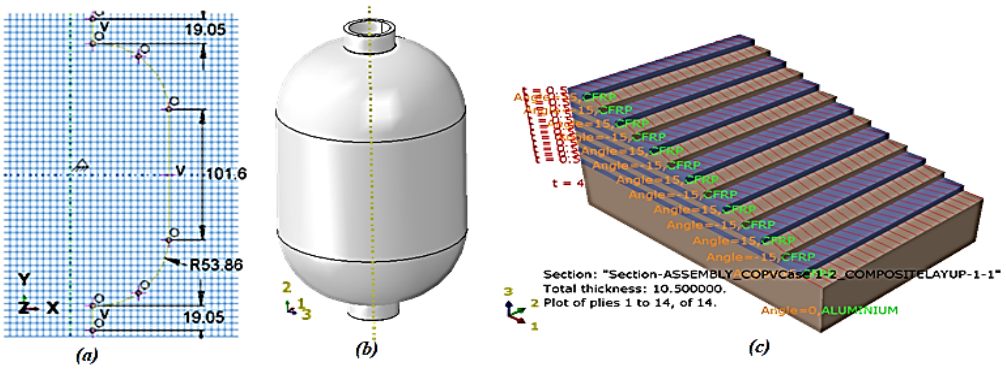

Figure 4. COPV: (**a**) Dimensions' layout, (**b**) 3D model of the linear, and (**c**) Stack sequence of lamina.

For the COPV, a composite lay-up consisting of 13 fundamental plies was created. When modeling the material properties of COPV in ABAQUS packages, engineering material attributes were added, and boundary conditions were created using the load module. The top face of the sectioned COPV was subjected to the boundary condition on *x*-axis (i.e., axis 1). Thus, the radial and circumferential displacements of COPV model were set to be in fixed position. The symmetric side faces were assigned to be boundary conditions on the *y*-axis (2) and the *z*-axis (3). Then, for the finite element optimum model iteration, the number of layers and layer sequence, the hoop angle, and the helical angle were varied in different scenarios to obtain a model that absorbs the maximum burst pressure. Using the load manager from the load module of ABAQUS software packages, a uniform pressure of 30 MPa was applied to the internal face. Figure 5 illustrates how mesh was created using quadratic hexahedral elements.

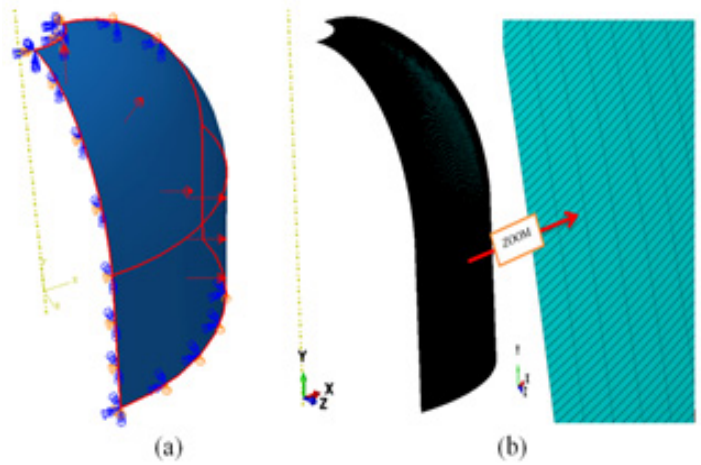

Figure 5. COPV FEM: (**a**) Boundary condition and loading (**b**) meshed model.

It is important to use different levels of mesh densities to ensure that FEM results can converge. Analyses with a coarse mesh may cause inaccurate results. The results of finite element simulations must converge to a fixed value by introducing mesh refinement. However, finite meshes lead to increased use of computational power. Therefore, finding the coarsest mesh that is still accurate enough is important. A mesh convergence study was carried out before proceeding to detailed analyses. For this purpose, four different mesh densities were used. For the present case, the S8R mesh generation element type was selected. The first model was used to analyze the convergence of the results. Figure 6 shows the models of four different mesh densities with the corresponding convergence results.

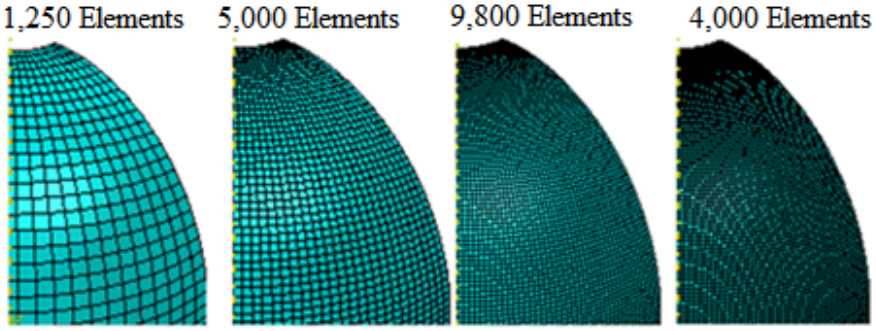

Figure 6. COPV implemented mesh densities for convergence study.

The computational study of the developed model was divided into two groups based on the fiber orientation and number of laminas employed in 14 COPV models. The maximum stress and strain, as well as Hashin's damage criterion, were used to com-

pute the developed burst pressure on each of the COPVs. The applied load was considered as the burst pressure at which the COPV was expected to fail when the failure index is greater than one. Figure 7 depicts a commonly used failure criterion evaluation approach that was employed in this study.

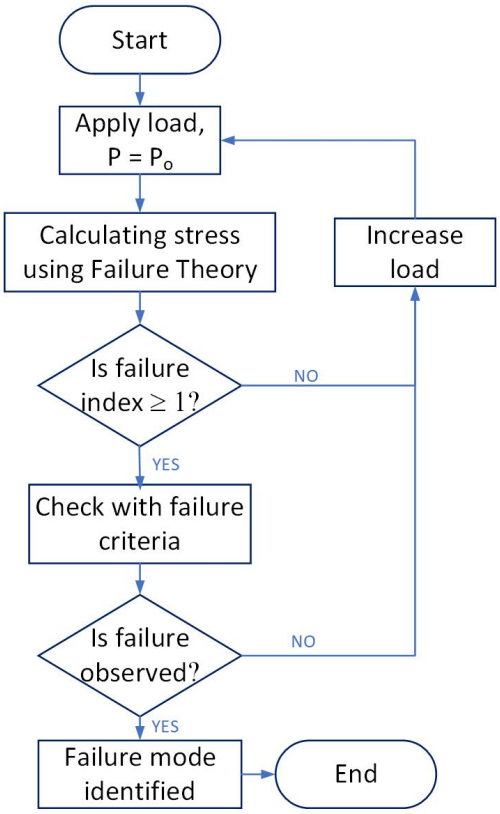

Figure 7. Flowchart of failure criterion.

The first 8 models were used to investigate the effect of orientation angle, while the next 6 models were used to investigate the effect of the layers. These numbers were selected randomly. For the first 8 models, the number of layers was taken from analytical approach analysis as 13 layers and changing the winding angle, and the internal pressure of 30 MPa was applied gradually with the small increments. The next 6 models (model 9–14) were analyzed by varying the number of layers without changing the orientation angle. In all models, the thickness of the composite was considered the same as the calculated value from the analytical approach, which is 6.5 mm.

3. Results and Discussion

The finite element models of the COPVs were created using S8R, and an eight-node thick curved shell with three-point integration components. The 3D models of the ASTM D 2585 vessel, as well as the composite lay-up, are shown in Figure 4a,b. The purpose of the computational study was to find the optimum winding angle for a COPV that could bear the highest burst pressure. Selecting the right mesh size is vital in achieving acceptable results with the least amount of processing resources. The chosen mesh sizes have an impact on the results of the computational study, where choosing a fine mesh will increase the number of the model's element-level computations, resulting in a high processing cost. As a result, finding the smallest mesh with an acceptable result was one of the approaches employed in this study. Therefore, a mesh convergence study was conducted prior to undertaking a detailed evaluation of the COPV models. The mesh sensitivity was also examined by varying the element sizes, with the final optimized mesh being employed in the analysis. The optimum composite overwrapped pressure vessel was obtained using

a total of 14 different models, as shown in Table 2. The mesh convergence analysis led to the selection of a COPV model built with 9800 elements as an input model for further simulation study.

Table 2. FEA-based burst pressure analysis results for ASTM2585 based COPV.

Case No.	No. of Layers	Winding Angle [°]/Ply Sequence	Calculated Burst Pressure Range (MPa)	Predicted Average Burst Pressure (MPa)
1	13	PP* [15, −15] s	-	-
2	13	PP [30, −30] s	-	-
3	13	PP [45, −45] s	19.7–20.5	20.1
4	13	PP [55, −55] s	20.7–27.756	24.228
5	13	PP [60, −60] s	17.7–24.75	21.225
6	13	HH** [75, −75] s	13.95–29.772	21.861
7	13	HH [89, −89] s	13.35–15.9	14.175
8	13	PHP [25/−25/87.5/−25/87.5/−25/87.5] s	-	-
9	5	PP [55, −55] s	20.115–28.515	24.315
10	8	PP [55, −55] s	21–27.99	24.495
11	14	PP [55, −55] s	20.7–27.9	24.3
12	20	PP [55, −55] s	20.859–27.759	24.309
13	21	PP [55, −55] s	20.706–27.756	24.231
14	27	PP [55, −55] s	20.8566–27.756	24.3063

P* stands for polar winding angle and H** stands for hoop winding angle.

The performance of the composite vessel is mostly determined by the toughness and strength of the composite layers, which are significantly related to the parameters of the fiber, the fiber's principle orientation, the stack sequence, and the geometrical size [34]. The model designated on the 10th case model shown in Table 2, which was designed with eight layers at a fiber orientation of [55°, −55°] s PP pattern, showcased an FEA-based result of a burst pressure of about 24.495 MPa and 20.1 MPa through an analytical method that performed as an optimal design alternative for the influence of the ply sequences evaluation for its stress bearing characteristics.

3.1. Burst Pressure Analysis

The failure load step value was observed to calculate the burst pressure by increasing the internal pressure by a small increment, where the critical burst pressure was obtained by multiplying the maximum internal target pressure set by the failure load step. To examine the failure index, based on the FEA report, the 10th model with eight layers of COPV plies bore a burst pressure of 24.495 MPa, which is indeed the optimum design for layering and sequencing the composite plies. This model was made with eight layers at [55°, –55°] and has a good combination for its maximum burst pressure, as can be seen from Table 2. According to the FEA results of models 1–3 and model 8, the failure index of the theoretical values is less than one. As a result, the failure pressure of COPVs is not determined by this load increment time step. The maximum strain failure indicators (MSTRN) for amplitudes of 0.925 and 0.93 are depicted in Figure 8. At a 0.93 amplitude, the MSTRN values are greater than one, as indicated in the large hoop part of the COPV half section. Accordingly, this load step duration is referred to as the failure pressure. At its amplitude, the burst pressure can be obtained or calculated as (0.93 × 30 MPa) = 27.9 MPa.

The maximum stress failure indices (MSTRS) are shown in Figure 9, in which it is shown that the maximum strain failure index is less than one for a 0.83-time frame-loading and larger than one for a 0.835-time frame-loading. This time frame failure index is a multiple of one and is found in the vessel's massive cylindrical section. As a result, the loading step time was used as a function to determine the burst pressure. According to the maximum stress failure criterion, at this step time, the burst pressure is (0.835 × 30 MPa) = 25.05 MPa.

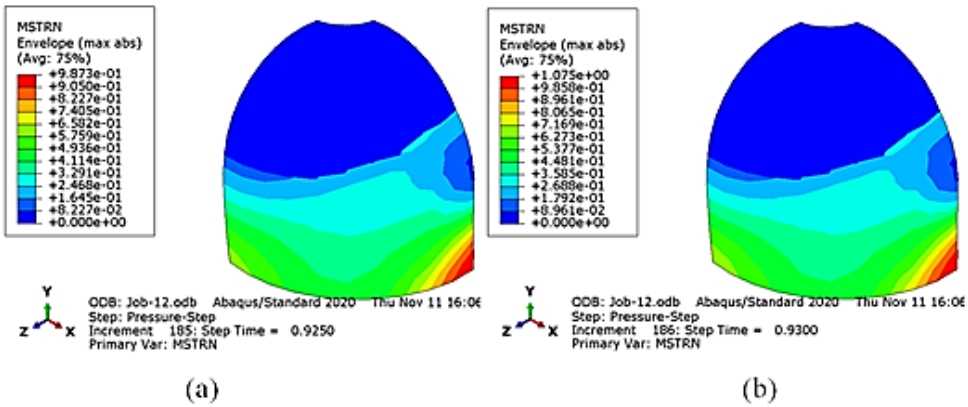

Figure 8. Maximum strain failure index: (**a**) at load step 0.925 and (**b**) at load step 0.93.

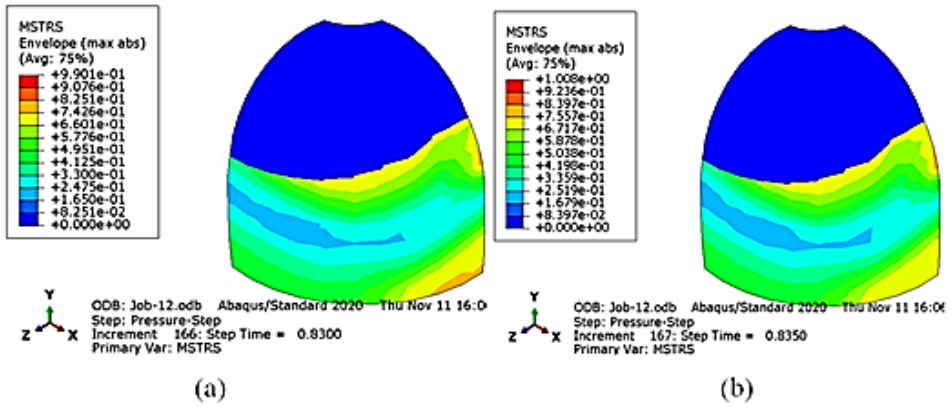

Figure 9. Maximum stress failure index: (**a**) lower than 1 at load step 0.83 and (**b**) greater than 1 at load step 0.835.

The Tsai–Hill failure indexes (TSAIH) are shown in Figure 10. As can be observed from Figure 10b, a major section of the vessel hoop portion has values greater than one at step time 0.7. At this step time, the calculated burst pressure is (0.7 × 30 MPa) = 21 MPa.

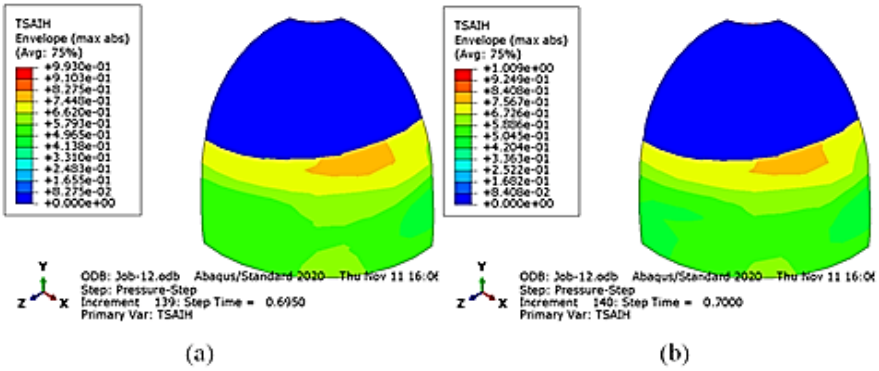

Figure 10. Tsai–Hill failure index (TSAIH): (**a**) lower than 1 at load step 0.695 and (**b**) greater than 1 at load step 0.7.

The model was also analyzed using the Tsai–Wu failure index (TSAIW), whose results for the step times 0.72 and 0.725 are shown in Figure 11. The TSAIW failure indices are lower than one in Figure 11a in all the areas of the model. Hence, this step time of the load is not considered as the burst pressure. However, in Figure 11b, the TSAIW contour at step time 0.725 is shown and the values are larger than one in the large hoop areas. This

increment loading is taken as the burst pressure. Thus, the burst pressure at this step time is (0.725 × 30 MPa) = 21.75 MPa.

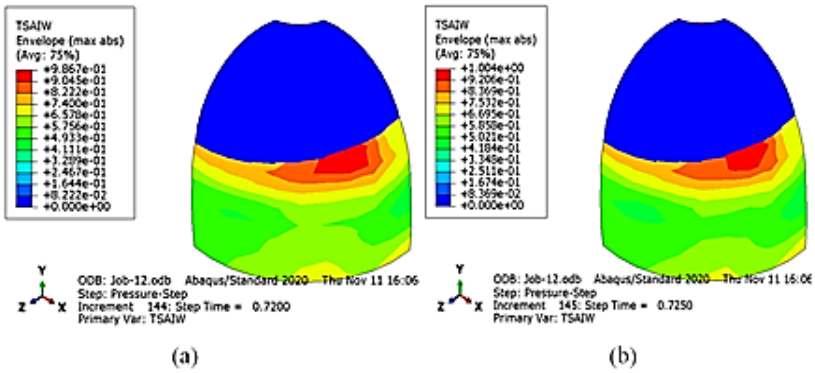

Figure 11. Tsai–Wu failure index: (**a**) lower than 1 at load step 0.72 and (**b**) greater than 1 at load step 0.725.

The Hashin fiber tension damage criterion (HSNFTCRT) contour plot is another composite material characterization criterion and the analysis performed on the model of this study is presented in Figures 12 and 13. The burst pressure was achieved when the Hashin fiber tension damage value exceeded one. Accordingly, Figure 13b illustrates the contour plot phenomenon of the HSNFTCRT that occurred at the loading step for a time frame of 0.76. At this point, the COPV fibers are completely damaged. Therefore, the burst pressure is equal to the loading increase. The burst pressure at this step time is (0.76 × 30 MPa) = 22.8 MPa.

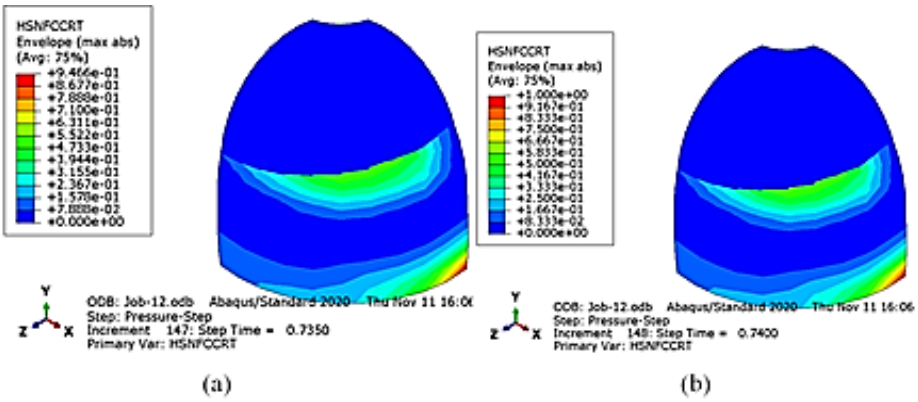

Figure 12. Hashin fiber compression failure index (HSNFCCRT): (**a**) lower than 1 at load step 0.735, and (**b**) greater than 1 at load step 0.74.

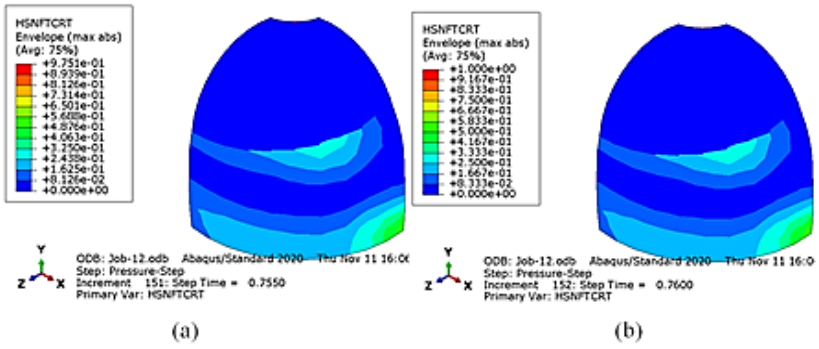

Figure 13. Hashin fiber tension failure index (HSNFTCRT): (**a**) lower than 1 at load step 0.755, and (**b**) greater than 1 at load step 0.76.

3.2. Effect of Stacking Sequence of Layers

According to the finite element study on the stacking sequence of composite plies, shown in Figure 4c for the construction of a COPV with identical ply thickness, there is no great difference in the induced burst pressure among the analyzed models. The numerical computation results on the COPV model for case 9 to case 14 with a fiber orientation at [55°, −55°] s revealed the significant effect of the ply quantity. Accordingly, the burst pressure varies as the number of plies varies. The maximum induced burst pressure for the researched models was found to be 24.495 MPa, which was induced on model case 10, whose details are given in Table 2. Figure 14 depicts a COPV made at a [55°, −55°] fiber orientation, with an inverse correlation between the burst pressure and plies quantities. As a result, as the ply quantity increases, the burst pressure falls.

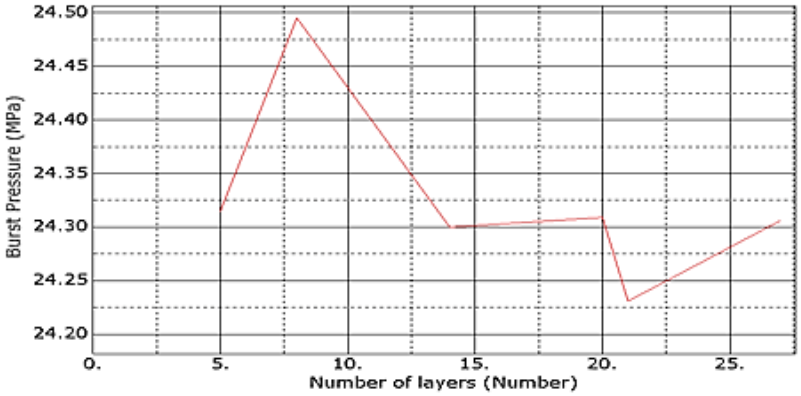

Figure 14. Effects of an increasing number of layers on burst pressure.

3.3. Fiber Angle Orientation Effect on Burst Pressure

An internal pressure in the continuous fiber enabled the composite pressure vessels to induce burst stress. Loading inconsistencies on pressure vessel structures lead to the formation of burst pressure and ruptures. Fiber breakage, inter-laminar matrix cracks, and interfacial cracks between plies can all result from a poor fiber orientation, resulting in catastrophic COPV failures. The burst pressure for the CFRP made the COPV pressure increase as the angle of orientation of the fiber increased, as indicated in Table 2. Figure 15 depicts the change in the burst pressure as a function of the fiber winding angle. Accordingly, the burst strength decreases as the fiber orientation increases. However, the optimum fiber winding angle for COPV is [55°, −55°].

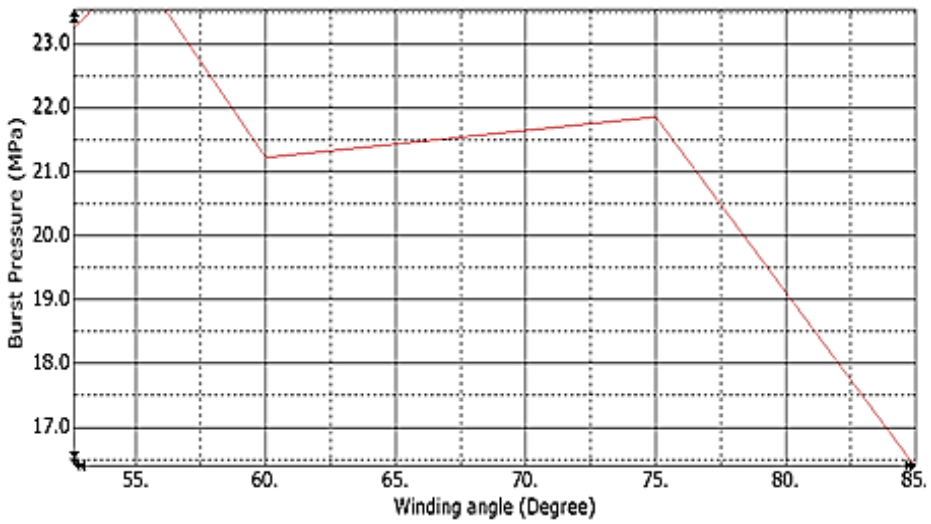

Figure 15. Variation of average burst pressure with winding angle.

3.4. Fiber Stress–Strain Distribution in the COPV

The pressure vessel's stress–strain response would determine its performance under any loading condition. In dealing with small elastic deformations, the linear model is frequently preferred. As a result, at elevated pressures, the displacement would surpass the elastic modulus, contradicting linear theory. Netting analysis has been used to predict stresses by different researchers [9,14,20]. The axial and hoop stress distributions of a multi-layered COPV varied depending on the fiber orientations as the ply quantity increased.

Fiber stress–strain values were extracted across the surface of the COPV, with the polar boss region having the highest stress–strain. As the boss approaches, the stress levels increase sharply, resulting in high stress gradients. This consideration is evident due to the variations in the composite thickness at various locations on the COPV. Figure 16 depicts the stress–strain effect variations for the case 10 model of this COPV study. According to the FEA, the maximum in-plane primary stress decreases up to 45° before rapidly increasing from 45° to 90°, as depicted in Figure 17.

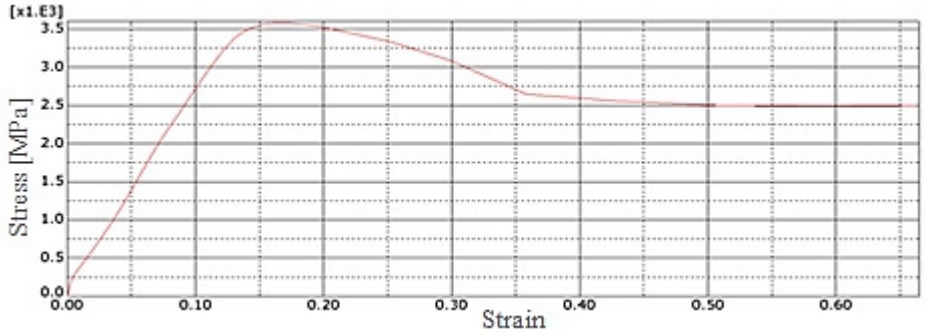

Figure 16. Variations of stress–strain for case 10 model.

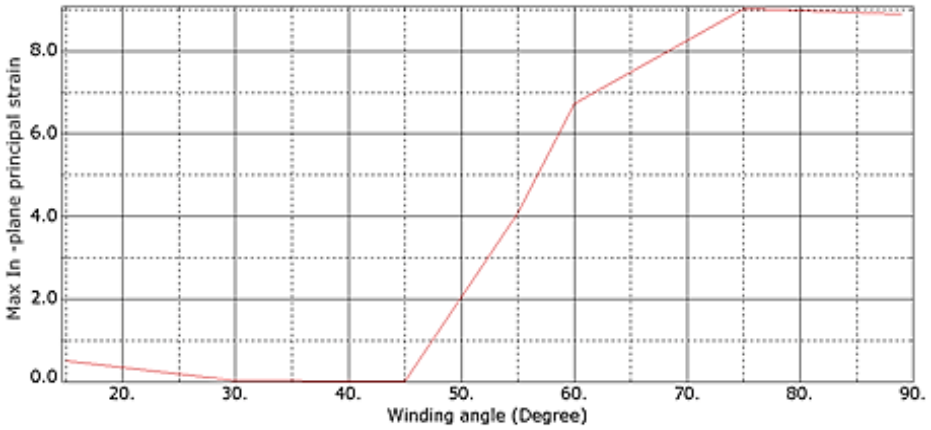

Figure 17. Variation of maximum principal strain with winding angle increase.

In the numerical analysis of the stress–strain profile of the composite structures, the Tsai–Wu failure theory found the burst pressure with more reliability [35]. Designs that use the tensile strength of fibres for resistance to loads caused by gases will outperform others [9]. Similar to other measurement variables, burst pressure is principally determined by the vessel material and the stored content dynamics or statics. The fiber strength rises as the fiber volume ratio rises, and so adopting the proper fiber orientation resulted in larger burst pressure accommodations. The three main factors that had to be taken into consideration when designing the COPV were the winding angle, the ply thickness, and the stacking sequence. These are necessary to generate an optimum and robust composite overwrapped pressure vessel for mitigating burst pressure issues. This is a lesson learned and to be expanded upon as a potential area of study for future researchers. The findings of the analysis and the FEA techniques utilized on 14 different models to determine the burst

pressure were determined to be acceptable. Utilizing the Tsai–Wu, Hashin, and maximum shear stress criteria, the maximum stress that caused the development of burst pressure was also established. The burst pressure that resulted in failure underwent a thorough analysis. The study included several scenarios with alternate stacking orders, different fiber orientations, and various ply thicknesses to illustrate how the COPV responds to internal pressure.

4. Conclusions

According to scholarly studies, the aviation industry uses the COPV principle for the development and production of solid rocket motor casings and rocket propellant tanks. Meanwhile, the steam producer and user industries benefit from the design and production of lightweight, high-pressure liquid storage tanks with the option of having a variety of inner lining materials. COPVs have also been commonly utilized as an efficient method of storing the highly compressed hydrogen required to drive green cars.

In a computation-based analysis of 14 models, two groups of COPV design case studies were used. A composite overwrapped pressure vessel with an internal pressure of 30 MPa entails the intended conditions that COPV models are expected to undergo in a performance evaluation. The performance indicators for the developed COPVs in both the constant and variable variants included the fiber orientation and ply sequence. Using FEA, the effect of the ply stacking order was examined for each proposed model, which had a variable fiber orientation but the same thickness. The optimum COPV design profile could bear a 24 MPa of burst pressure with eight plies of carbon fiber and a [55°, −55°] PP winding pattern. The FEA method was also used to determine the distribution of stress and strain along the shape of the COPV. It was found that the distribution was constant over the surface of the COPV and that its highest values were observed in the polar boss area. As the boss prepared to advance geometrically into the dome phase, extreme stress gradients were observed.

When modeling and simulating the COPV type IV with an inner liner made of aluminum 6061 class in ABAQUS/CAE, the researchers used ASTM D2585 standards. Each of the COPV models were rigorously designed and individually analyzed while accounting for varying the fiber orientations and a set number of plies and sequences. A [55°, 55°] s PP fiber orientation pattern is the optimum COPV design out of the eight models that were constructed and independently tested for the case-1 study category. In accordance with other scholars' findings, the fiber orientation at an angle of [55, −55] s was the better fiber orientation that could withstand the maximum burst pressure of the cylindrical COPV.

For determining the COPV's failure mode, many techniques were used to develop various failure criteria. Many scholars prefer to analyze composite structure failure using the Hashin damage initiation criterion due to the polynomial-based Tsai–Hill and Tsai–Wu criteria's single equation for damage initiation prediction. As a result, when studying the failure of the fiber and matrix used in the design of COPVs, the Hashin damage initiation criterion was taken into consideration. In addition, the burst pressure of the inner liner was estimated using the maximum stress failure criterion, and the burst pressure of the composite part was determined using the Tsai–Wu failure criterion. Furthermore, the burst pressure calculated using the maximum stress and strain criteria is more conservative, whereas the Hashin damage criterion produces a high value, which could indicate that it is an optimum failure index of the COPV damage initiation. For the advanced design and production of COPVs with optimum structural integrity, more emphasis should be placed on the netting design and the analysis of the fiber winding angle, ply thickness, manufacturing techniques, and novel fiber or lamina bonding materials.

Author Contributions: Conceptualization, Y.R. and J.G.; methodology, J.G. and Y.R.; software, J.G.; validation, Y.R. and H.G.L.; formal analysis, J.G. and Y.R.; investigation, J.G. and Y.R.; resources, Y.R. and H.G.L.; data curation, Y.R.; writing—original draft preparation, Y.R. and J.G.; writing—review and editing, H.G.L.; visualization, Y.R. and H.G.L.; supervision, Y.R. and H.G.L.; project administration, Y.R.; funding acquisition, Y.R. and H.G.L. All authors have read and agreed to the published version of the manuscript.

Funding: This research received no external funding.

Institutional Review Board Statement: Not applicable.

Informed Consent Statement: Not applicable.

Data Availability Statement: Not applicable.

Conflicts of Interest: The authors declare no conflict of interest.

References

1. Andrianov, A.; Tomita, E.K.; Veras, C.A.G.; Telles, B. A Low-Cost Filament Winding Technology for University Laboratories and Startups. *Polymers* **2022**, *14*, 1066. [CrossRef]
2. Li, G.; Yan, Z.; Outer, B.; Creep, R.; Load, G. Model assessment of the lifetime of a composite overwrapped pressure vessel under creep conditions. *J. Phys. Conf. Ser.* **2020**, *1666*, 012069. [CrossRef]
3. Thesken, J.C.; Palko, J.L.; Eldridge, J.; Sutter, J. *A Theoretical Investigation of Composite Overwrapped Pressure Vessel (COPV) Mechanics Applied to NASA Full Scale Tests*; NASA Center for Aero Space Information (CASI): Hanover, MD, USA, 2009.
4. Schonberg, W.P. A rupture limit equation for pre-loaded laminated composite plates. *J. Compos. Sci.* **2018**, *2*, 3. [CrossRef]
5. Sofi, T.; Neunkirchen, S.; Schledjewski, R. Advanced manufacturing: Polymer & Composites Science Path calculation, technology and opportunities in dry fiber winding: A review. *Adv. Manuf. Polym. Compos. Sci.* **2018**, *4*, 57–72. [CrossRef]
6. Regassa, Y.; Lemu, H.G.; Sirhabizu, B. Burst strength analysis of composite overwrapped pressure vessel using finite element method. *IOP Conf. Ser. Mater. Sci. Eng.* **2021**, *1201*, 012029. [CrossRef]
7. Forth, S.C.; Pat, B. *Composite Overwrapped Pressure Vessels, a Primer*; NASA Center for Aero Space Information: Hanover, MD, USA, 2011.
8. Azeem, M.; Haji, H.; Kumar, M. Application of filament winding technology in composite pressure vessels and challenges: A Review. *J. Energy Storage* **2022**, *49*, 103468. [CrossRef]
9. Jois, K.C.; Welsh, M.; Gries, T.; Sackmann, J. Numerical analysis of filament wound cylindrical composite pressure vessels accounting for variable dome contour. *J. Compos. Sci.* **2021**, *5*, 56. [CrossRef]
10. Alam, S.; Yandek, G.R.; Lee, R.C.; Mabry, J.M. Design and development of a filament wound composite overwrapped pressure vessel. *Compos. Part C* **2020**, *2*, 100045. [CrossRef]
11. Hastie, J.C.; Kashtalyan, M.; Guz, I.A. Analysis of filament-wound sandwich pipe under combined internal pressure and thermal load considering restrained and closed ends. *Int. J. Press. Vessel. Pip.* **2021**, *191*, 104350. [CrossRef]
12. Madhavi, M.; Rao, K.V.J.; Rao, K.N. Design and analysis of filament wound composite pressure vessel with integrated-end domes. *Def. Sci. J.* **2009**, *59*, 73–81. [CrossRef]
13. Barthelemy, H.; Weber, M.; Barbier, F. Hydrogen storage: Recent improvements and industrial perspectives. *Int. J. Hydrogen Energy* **2017**, *42*, 7254–7262. [CrossRef]
14. Sahami, M.; Heidary, H. Parametric study on drilling of GFRP composite pipe produced by fi lament winding process in different backup condition. *Compos. Struct.* **2020**, *243*, 111661. [CrossRef]
15. Trzepieciński, T.; Najm, S.M.; Sbayti, M.; Belhadjsalah, H.; Szpunar, M.; Lemu, H.G. New advances and future possibilities in forming technology of hybrid metal–polymer composites used in aerospace Applications. *J. Compos. Sci.* **2021**, *5*, 217. [CrossRef]
16. Luca, S.; Emmanouel, A.; Costanzo, B. Robotic filament winding: An innovative technology to manufacture complex shape structural parts. *Compos. Struct.* **2019**, *220*, 699–707. [CrossRef]
17. Zu, L.; Xu, H.; Jia, X.; Zhang, Q.; Wang, H.; Zhang, B. Winding path design based on mandrel profile updates of composite pressure vessels. *Compos. Struct.* **2020**, *235*, 111766. [CrossRef]
18. Krysiak, P.; Błachut, A.; Kaleta, J. Theoretical and experimental analysis of inter-layer stresses in filament-wound cylindrical composite structures. *Materials* **2021**, *14*, 7037. [CrossRef]
19. Bari, K.; Bollenbach, L. Spiderweb cellular structures manufactured via additive layer manufacturing for aerospace application. *J. Compos. Sci.* **2022**, *6*, 133. [CrossRef]
20. Nguyen, B.N.; Simmons, K. A multiscale modeling approach to analyze filament-wound composite pressure vessels. *J. Compos. Mater.* **2013**, *47*, 2113–2123. [CrossRef]
21. Canal, J.P.; Micuzzi, A.; Logarzo, H.; Terlisky, A.; Toscano, R.; Dvorkin, E. On the finite element modeling of COPVs. *Comput. Struct.* **2019**, *220*, 1–13. [CrossRef]
22. Hugaas, E.; Vedvik, N.P.; Echtermeyer, A.T. Progressive fatigue failure analysis of a filament wound ring specimen with a hole. *J. Compos. Sci.* **2021**, *5*, 251. [CrossRef]

23. Tarakcioglu, N.; Samanci, A.; Arikan, H.; Akdemir, A. The fatigue behavior of (±55°) 3 filament wound GRP pipes with a surface crack under internal pressure. *Compos. Struct.* **2007**, *80*, 207–211. [CrossRef]
24. Hu, J.; Chen, J.; Sundararaman, S.; Chandrashekhara, K. Analysis of composite hydrogen storage cylinders subjected to localized flame impingements. *Int. J. Hydrogen Energy* **2008**, *33*, 2738–2746. [CrossRef]
25. Halawa, M.; Al-Huniti, N. Optimum design of carbon/epoxy composite pressure vessels including moisture effects. *J. Compos. Sci.* **2019**, *3*, 65. [CrossRef]
26. Alam, S.; Divekar, A. Design optimisation of composite overwrapped pressure vessel through finite element analysis. In Proceedings of the ASME IMECE2017, Tampa, FL, USA, 3–9 November 2017; Volume 9. [CrossRef]
27. Kamal, A.M.; El-Sayed, T.A.; El-Butch, A.M.A. Analytical and finite element modeling of pressure vessels for seawater reverse osmosis desalination plants. *Desalination* **2016**, *397*, 126–139. [CrossRef]
28. Henrietta, W.L.; Nicolaas, E.; Phillimon, M.M.; Dmitri, B. *Chapter 13—Hydrogen Storage, Electrochemical Power Sources: Fundamentals, Systems, and Applications*; Smolinka, T., Garche, J., Eds.; Elsevier: Amsterdam, The Netherlands, 2022; pp. 455–486. [CrossRef]
29. Sulaiman, S.; Borazjani, S.; Tang, S.H. Finite element analysis of filament-wound composite pressure vessel under internal pressure. *IOP Conf. Ser. Mater. Sci. Eng.* **2013**, *50*, 012061. [CrossRef]
30. Kartav, O.; Kangal, S.; Yücetürk, K.; Tanoğlu, M. Development and analysis of composite overwrapped pressure vessels for hydrogen storage. *J. Compos. Mater.* **2021**, *55*, 4141–4155. [CrossRef]
31. Wang, H.; Fu, S.; Chen, Y.; Hua, L. Thickness-prediction method involving tow redistribution for the dome of composite hydrogen storage vessels. *Polymers* **2022**, *14*, 902. [CrossRef]
32. Kang, H.; He, P.; Zhang, C.; Dai, Y.; Lv, H.; Zhang, M.; Yang, D. Stress–strain and burst failure analysis of fiber wound composite material high-pressure vessel. *Polym. Polym. Compos.* **2021**, *29*, 1291–1303. [CrossRef]
33. Sulaiman, S.; Borazjani, S.; Roshanand, A.; Heydaryan, S. Failure analysis of aluminum reinforced composite vessel. *Appl. Mech. Mater.* **2014**, *392*, 178–182. [CrossRef]
34. Nikbakt, S.; Kamarian, S.; Shakeri, M. A review on optimization of composite structures Part I: Laminated composites. *Compos. Struct.* **2017**, *195*, 158–185. [CrossRef]
35. Kumar, S.S.; Kumari, A.S. Design and Failure analysis of Geodesic Dome of a Composite Pressure vessel. *Int. J. Eng. Technol.* **2012**, *1*, 1–8.